Oceanic Lidar Operating at High Altitudes: a Computer Model Study

B. Bartsch*, T. Braeske and R. Ruter

University of Oldenburg Physics Department 2900 Oldenburg, Germany

ABSTRACT

The presented computer model study considers an oceanic lidar operating at high altitudes under daylight conditions, measuring concentrations of gelbstoff and chlorophyll in the surface layer of the sea. Only a cloudless and stratified atmosphere is taken into account. Emission of the illuminated seawater is investigated in the wavelenght region of water Raman scattering and fluorescence of gelbstoff and chlorophyll.

The chosen laser and sensor specifications are: 1 J output energy, 10 ns pulse duration, 0.1 mrad beam divergence, 0.1 mrad detection angle. Signal recovery is carried out over the effective pulse lenght of the returned signal, which is roughly 20 -30 ns.

As a result of the study the recommended excitation wavelenght interval for high altitudes should be chosen between 350 and 400 nm. Under these circumstances oceanic lidar measurements should be possible also at flight attitudes of up to 100 km under clear visibility conditions and with the given laser and sensor specifications even at noon.

INTRODUCTION

Oceanic parameters like the concentrations of gelbstoff and chlorophyll can be measured from the inelastic spectrum of seawater with excitation in the near UV or VIS (Fig. 1). By normalizing the fluorescence signals to water Raman scattering concentrations of gelbstoff and chlorophyll in relative units are derived.

Today these spectra are measured from low-flying aircraft without any necessity to correct the atmospheric influence on the measured signal.

However, the relevance of oceanic lidar would be highly improved if flight altitudes of more than 10 km could be achieved, since this would yield an essential improvement of the pixel coverage on the ground. Two main problems have to be investigated: (i) the influence of the atmosphere, as a function of parameters which determine the atmospheric transmission like the aerosol and ozone distributions, and (ii) the Signal to background ratio which has to be high enough for signal recovery also during daytime measurements.

To study the possibility of operating an oceanic lidar from high altitudes, computer simulations of the radiative transfer were peformed with various viewing gometries of the lidar with respect to the sun elevation. The considered wavelengt interval ranges from 300 to 700 nm. The atmosphere is assumed to be cloudless and stratified.

1. RADIATIVE TRANSFER IN THE ATMOSPHERE

1.1 Laser induced signal

For the calculations of the laser induced signal the Raman and fluorescence lidar equtions are used, which are integrated over a water layer reaching from the surface to a water depth z_0 which corresponds to two attenuation lengths at the laser wavelength.

In the Raman lidar equation the Raman backscattering cross section of water is needed. Denoting the angle between the scattering direction and the polarization direction of the incoming beam with α, published data of the differential Raman scattering cross section of water σ_R (λ_{ex}, α) vary from $8.1 \cdot 10^{-30}$ to $4.5 \cdot 10^{-29}$ $cm^2\ sr^{-1}$ $molecule^{-1}$, where the excitation wavelength λ_{ex} is chosen to 488 nm and α to 90° (Marshall and Smith, 1990). With the definition of α in mind the water Raman backscattering coefficient for polarized and also fr unpolarized laser radiation is given by the above

* now: University of Hamburg, Institute of Oceanography, 2000 Hamburg 54, Germany.

values of σ_R (λ_{ex}, $\alpha = 90°$). The wavelength dependence of the Raman cross section is given by the λ_{ex}^{-4} law.
For calculating the fluorescence signal we use three fluorescence spectra of North Sea water (Fig. 1), measured during an experiment in 1990.

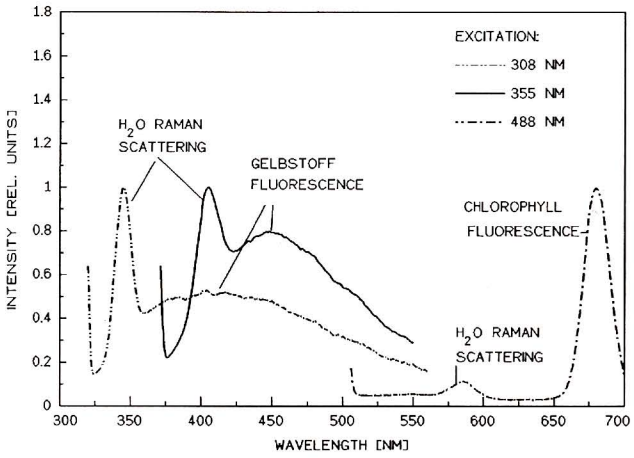

Fig. 1 - Fluorescence spectra of North Sea water for three excitation wavelengths.

Attenuation data of the same sample are also available. The spectra were measured in a direction perpendicular to the incoming beam which was unpolarized. Therefore the measured Raman signals have to be converted into Raman backscattering signals by a formula of SchrÖtter (1979) which describes the dependence of the Raman scattering cross section on the above defined angle α

$$\sigma_R(\lambda_{ex}, \alpha) = \sigma_R(\lambda_{ex}, 90°) \cdot \frac{2\rho + (1-\rho)\sin^2\alpha}{1+\rho} \qquad (1)$$

with the depolarisation factor $\rho = 0.17$.
By normalizing the measured fluorescence signals to the converted water Raman scattering intensity one calculates absolute values for Raman and fluorescence signals.

1.2 Solar background

For calculating the solar background, which is measured from a flying platform, one divides the solar induced signal into four terms:
- the path radiance, describing contributions which are scattered to the sensor within the atmosphere,
- the sun-glitter radiance, originating from direct sunlight reflected by the water surface into the viewing field of the sensor,
- the sky-glitter radiance, representing diffuse sunlight which is reflected by the water surface into the viewing field of the sensor, and
- the wather leaving radiance, emerging from the sea bulk and reaching the sensor. These four terms which describe the solar background of the lidar signal are calculated from formulas of Guzzi et al. (1987).

1.3 Fuxed values of the model

Molecules and aerosols are the main atmospheric constituents affecting the radiation in the wavelength interval between 350 and 700 nm. At wavelengths below 350 nm ozone absorption becomes a dominating factor. However, only the attenuation through molecules - the Rayleigh scattering - is a fixed parameter, whereas the others are highly variable.
The optical depth $\tau(\lambda, h)$ is defined as

$$\tau(\lambda, h) := \int_0^h k(\lambda, h')\, dh' \qquad (2)$$

where $\kappa(\lambda,h')$ is the attenuation coefficient of the considered attenuation process, λ the wavelength and h the height above the surface. Therefore the transmission $T(\lambda,h)$ from the surface to height h can be expressed by

$$T(\lambda, h) := e^{-\tau(\lambda, h)/\cos\theta} \qquad (3)$$

where θ denotes the incidence angle of the incoming radiation.
Rayleigh scattering was investigated by various authors. The results are corresponding well with each other.
Our calculations are based on the formula of Frohlic and Shaw (1980), which describes the Rayleigh optical depth of the whole atmosphere.
Also the molecule distribution with height is well known (van Stokkom and Guzzi, 1984).
This results in the Rayleigh optics depth of a layer reaching from the surface to the height h given by

$$\tau_R(\lambda, h) = H_R(h) \cdot \tau(\lambda, \infty) \qquad (4)$$

where $H_R(h)$ is the so-called relative optical depth with

$$H_R(h) = 1 - e^{(-0.1188 \cdot h - 0.00116 \cdot h^2)} \qquad (5)$$

(van Stokkom and Guzzi, 1984) and

$$\tau(\lambda, \infty) = 0.0038 \cdot \lambda^{-(3.916 + 0.074 \cdot \lambda + 0.050/\lambda)} \qquad (6)$$

(Fröhlich and Shaw, 1980), thus the Rayleigh optical depth almost decreases with the fourth power of the wavelength.
Another fixed input parameter is the extraterrestrial solar spectrum of which values are listed by Thekekara (1973). There also exists a formula given by Green and Schippnick (1982) which covers the wavelength region from 280 to 380 nm.

2. INPUT PARAMETERS OF THE MODEL

2.1 Aerosol scattering

Besides the flight height, the excitation and detection wavelengths and besides the zenith angles of the sun and the sensor, the most variable input parameter of the model is the scattering on aerosols within the atmosphere.
Shettle and Fenn (1976) show profiles of the attenuation coefficient at 550 nm for a wide range of atmospheric conditions (Fig. 2).

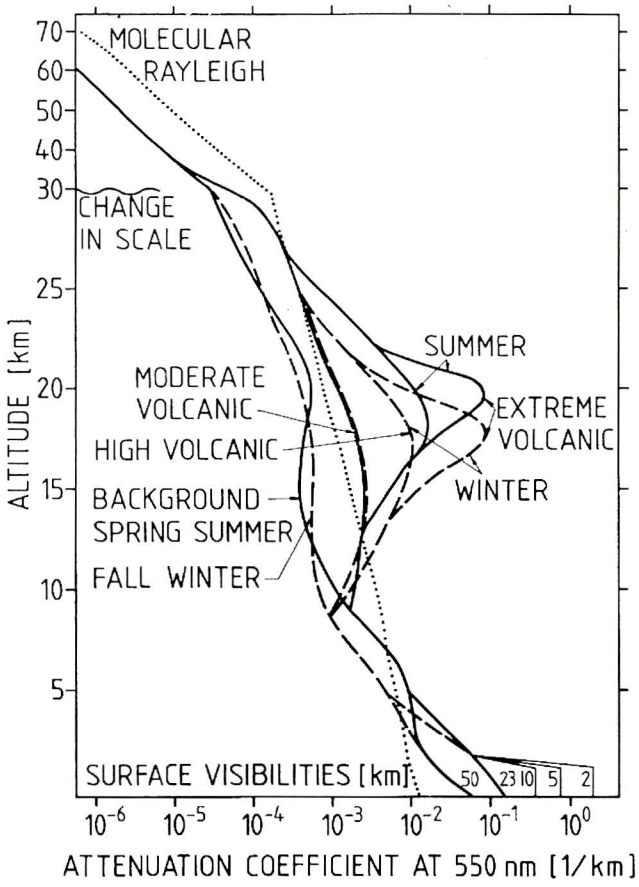

Fig. 2 - Vertical distribution of the aerosol attenuation coefficient at 550 nm (Shettle and Fenn, 1976).

The coefficients depend on the season and the amount of vulcanic dust in the stratosphere. Within the first two kilometres they also depend on the surface visibility.
Although wind velocity and relative humidity also influence the scattering on aerosols within the first 100 m, they are not taken into consideration in Fig. 2 According to Shettle and Fenn the data are valid for moderate wind velocity and a relative umidity of 80 %.
As the scale to the right is logarithmic, the surface visibility has the most important influence on the optical depth of aerosols, except in regions with extreme vulcanic conditions.
There also exist various graphics (Shettle and Fenn, 1976) which show the changes of the attenuation coefficient with wavelength in dependence of the considered surface remon (like maritime, urban and rural) and the considered layer of altitude. In the considered wavelength interval the optical depth of aerosols sligktly decreases with wavelength.

2.2 Ozone absorption

Another attenuation process in the atmosphere is the absorption through ozone, which is highly variable in the wavelength interval between 200 and 350 nm.
In Fig. 3 the optical depth resulting from ozone absorption in dependence of wavelength for various amounts of ozone is shown (Green and Schippnick, 1982; Vigroux, 1953).

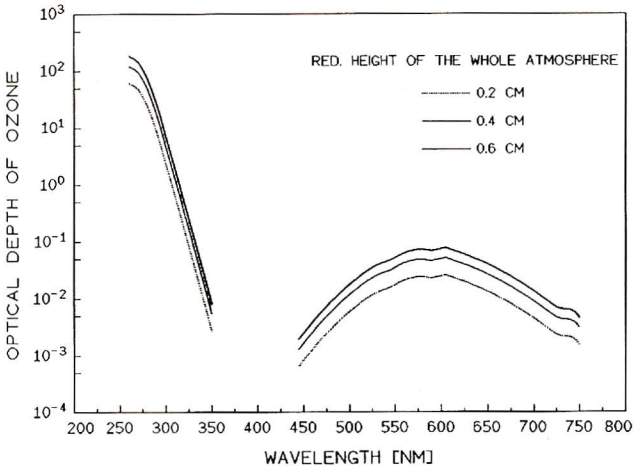

Fig. 3 - Optical depth of ozone absorption of the whole atmosphere for various amounts of ozone.

As can be seen, the absorption in the region from 260 to 320 nm is very high and decreases by four orders of magnitude between 260 and 350 nm. Between 350 and 450 nm the absorption through ozone can be neglected, whereas at higher wavelengths there is another band of absorption which is, however, weak so that in the wavelength interval from 350 to 700 nm absorption through ozone is nearly a fixed value.
For our calculations also the amount of ozone in the whole atmosphere and the relative optical depth of layers from the surface to various heights with respect to the whole atmosphere are needed. As an average value for the reduced height of ozone of the whole atmosphere 0.3 cm is chosen.

The distribution with height is described by a formula of Green (1964), from which it is concluded that the main part of ozone is located between 10 and 35 km altitude.

2.3 Subsurface albedo

Furthermore for the solar background the subsurface albedo of the ocean in dependence of the amount of gelbstoff and chlorophyll must be considered. This part of the radiative transfert model can be described by formulas of Morel and Prieur (1977) and Baker and Smith (1982). However, as can be seen in this model the variability of the subsurface albedo has only a small influence on the measured signal at high altitudes.

3. THE SOLAR INDUCED SIGNAL

3.1 Validation the model

For validation of the model parameters, the calculated downwelling solar irradiance at the earth's surface is compared with measurements made by Kok (1972). His measurements of the downwelling solar irradiance on a horizontal surface of the earth were made at Pretoria at clear weather conditions. The zenith angle of the sun was 60°. Fig. 4 shows the measured and our calculated data, where we have chosen the reduced height of ozone of the whole atmosphere at Pretoria to 0.26 cm and the total albedo of the earth's surface to 0.20. The model values agree very well with the measured data.

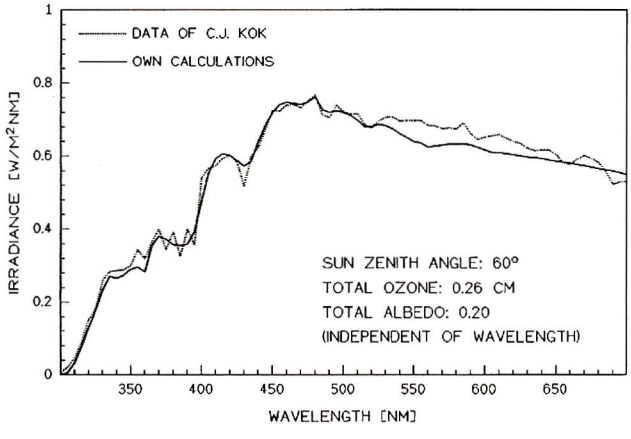

Fig. 4 - Measured (Kok, 1972) and calculated downwelling irradiance on a horizontal surface of the earth at Pretoria.

3.2 The solar background

Now a flying platform is considered with a sensor looking down to the ocean and measuring upwelling solar radiance. The registered spectrum is calculated for oceanic conditions.

Fig. 5 shows the calculated solar radiance (sun zenith angle: 30°, sensor zenith angle: 0°, surface visiblity: 10 km, reduced height of ozone: 0.3 cm.

As a result of the sharp decrease of absorption through ozone in the region from 260 to 350 nm, the solar radiance increases very strongly up to 350 nm.

At higher wavelengths the changes in the radiance are smoother.

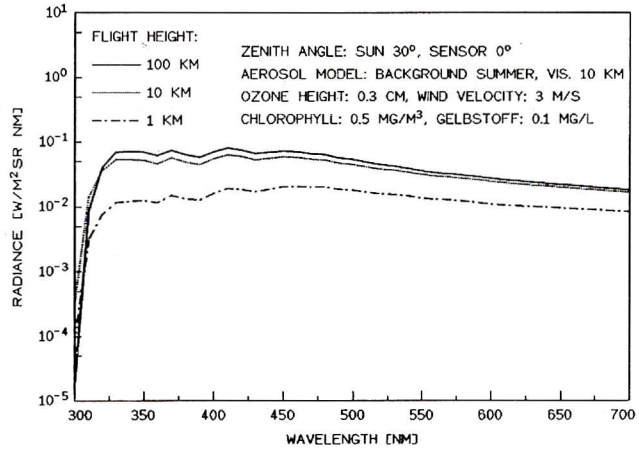

Fig. 5 - Solar radiance measured by a sensor looking to the ocean.

It is also obvious, that the radiance increases with flight height except in those regions where the absorption through ozone is very strong.

4. LASER INDUCED SIGNAL VERSUS SOLAR BACKGROUND

For the calculation of the laser induced signal, the following laser and sensor specifications were chosen: 1 J output energy, 10 ns pulse duration, 0.1 mrad beam diver gence, 0.1 mrad detection angle. Signal recovery is carried out over the effective pulse length of the returned signal, which is roughly 20 - 30 ns.

Three excitation wavelengths are chosen: 308 and 355 nm for excitation of gelbstoff fluorescence and 488 nm for excitation of chlorophyll fluorescence.

For each laser wavelength for detection wavelengths are chosen: three fluorescence wavelengths and the corresponding Raman scattering wavelength.

Figs. 6 - 8 show the laser induced signals and the solar background for three flight heights of 0.3, 10 and 100 km. Squares refer to 308 nm excitation, circles to 355 and triangles to 488 nm excitation. The signals at 345, 405 and 586 are the net water Raman scattering signals without any underlying gelbstoff or chlorophyll fluorescence. The crosses refer to the solar background.

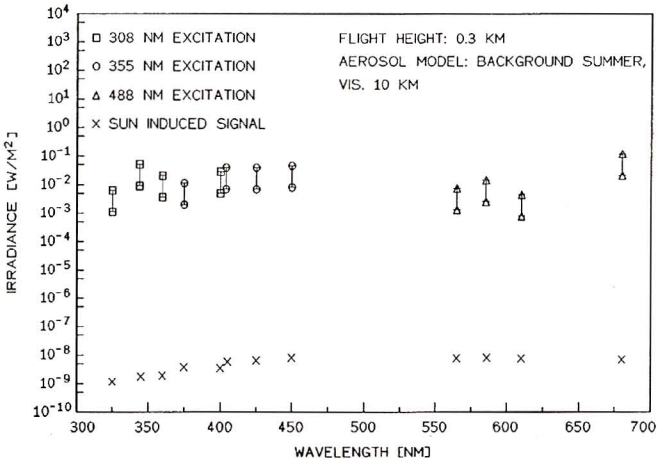

Fig. 6 - Laser induced signals for three excitation wavelengths and solar background at 300 m flight height.

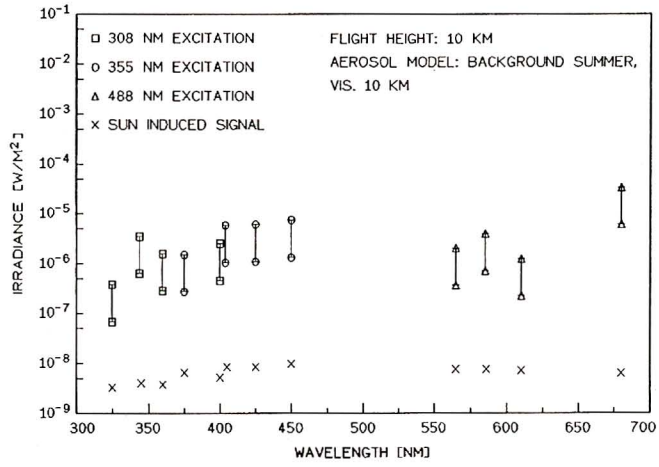

Fig. 7 - Laser induced signals for three excitation wavelengths and solar background at 10 km flight height.

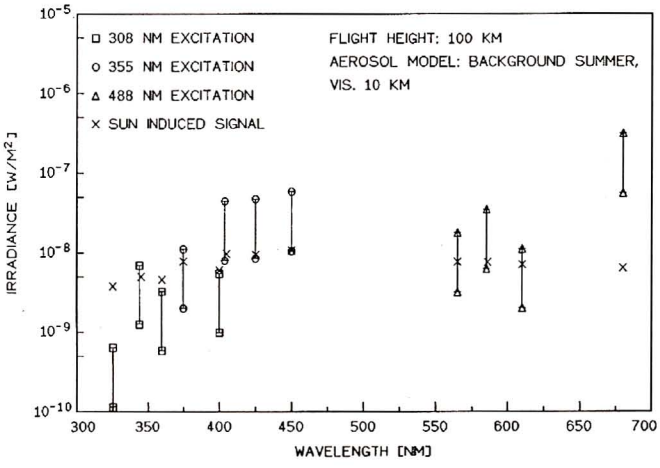

Fig. 8 - Laser induced signals for three excitation wavelengths and solar background at 100 km flight height.

The chosen model parameters are: sun and sensor at the zenith, that means the worst conditions of daylight measurements, reduced height of ozone: 0.3 cm, surface visibility: 10 km.
The great error bars given for the laser induced signals are caused by the wide range of Raman srattering cross sections in the literature. As can be seen in Fig. 6 lidar measurements with the given laser specifications are possible without any problems even at noon at 300 m flight height. With 10 km flight height (Fig.7) the laser iduced signals are still one or two orders higher than the solar background. A flight height of 100 km (Fig. 8) results in laser and solar induced signals of the same order.
Therefore at clear weather conditions oceanic lidar measurements are possible up to flight heights of 100 km even at noon. For higher altitudes or bad weather conditions lidar measurements are only possibly at night.
Excitation wavelengths below 350 nm are not very efficient if one measures at high altitudes. For example, the 308 nm laser radiation (Fig. 8) is strongly absorbed through ozone on its way to the surface. Excitation wavelengths above 400 nm will lead to restrictions because of eye safety. For these reasons one has to choose the excitation wavelength between 350 and 400 nm, for example the triple Nd-YAG laser wavelength at 355 nm.

CONCLUSIONS

It has been shown that for clear weather conditions oceanic lidar measurements are possible up to flight heights of 100 km even at noon.
The necessary laser specifications are: 1 J output energy, 10 ns pulse duration, about 20 - 30 ns detection time, 0.1 mrad beam and detection divergence.
The recommended excitation wavelength interval reaches from 350 to 400 nm. This includes 355 nm, the tripled Nd--YAG laser wavelength.
For higher altitudes or bad weather conditions the signal to background ratio must be increased by improving the laser specifications in order to make daylight measurements possible.

REFERENCES

Baker, K.S. and Smith, R.C., 1982, Bio-optical classification and model of natural waters. Limnology and Oceanography, 27, 3, pp. 500 -509.

Fröhlich, C. and Shaw, G.E., 1980, New Determination of Rayleigh Scattering in the Terrestrial Atmosphere. Appl. Optics, 19, 11.

Green, A.E.S., 1964, Attenuation by Ozone and the Earth's Albedo in the Middle Ultraviolet. Appl. Optics, 3, 2.

Green, A.E.S. and Schippnick, P.F., 1982, "UV-B Reaching the Surface" in the Role of Solar UV Radiation in Marine Ecosystems, ed. J. Calkins (New York and London: Plenum Press).

Guzzi, R., Rizzi, R. and Zibordi, G., 1987, Atmospheric correction of data measured by a flying platform over the sea: elements of a model and its experimental validation. Appl. Optics, 26, 15.

Kok, J.C., 1972, Spectral Irradiance of Daylight for Air Mass 2. J. Phys. D: Appl. Phys., 5.

Marshall, B.R. and Smith, R.C., 1990, Raman Scattering and In-Water Ocean Optical Properties. Appl. Optics, 29.

Morel, A. and Prieur, L., 1977, Analysis of variations in ocean color. Limnology and Oceanogaphy, 22, 4, pp. 709 - 722.

Schrötter, H.VV. and Klockner, H.VV.,1979, "Raman Scattering Cross Sections in Gases and Liquids" in: Raman Spectroscopy of Gases and Liquids (Berlin: Springer Verlag, pp. 123-166).

Shettle, E.P. and Fenn, R.VV., 1976, Models of the atmopsheric aerosols and their optical properties. AGARD Conf. proc. 183. available from U.S. NTIS (Springfield, Va. 22151) AD A028-615.

Stokkom, Van H.T.C. and Guzzi, R., 1984, Cover Airborne MSS data processing for forest classification. Int. J. Remote Sensing, 5, 6, 925 -938.

Thekaekara, M.P., 1973, Solar energy outside the earth's atmosphere. Solar energy, 14, pp. 109 - 127.

Vigroux, E., 1953, Contribution a l'tude exprimentale de l'absorption de l'ozone. Ann. Phys. 12, 8, pp. 709 - 762.